IEEE Photonics Journal
An IEEE Photonics Society Publication

Open Access

Optical Gaussian Notch Filter Based on Periodic Microbent Fiber Bragg Grating

Volume 6, Number 1, February 2014

M. M. Ali, Student Member, IEEE
K. S. Lim, Member, IEEE
A. Becir
M. H. Lai
H. Ahmad

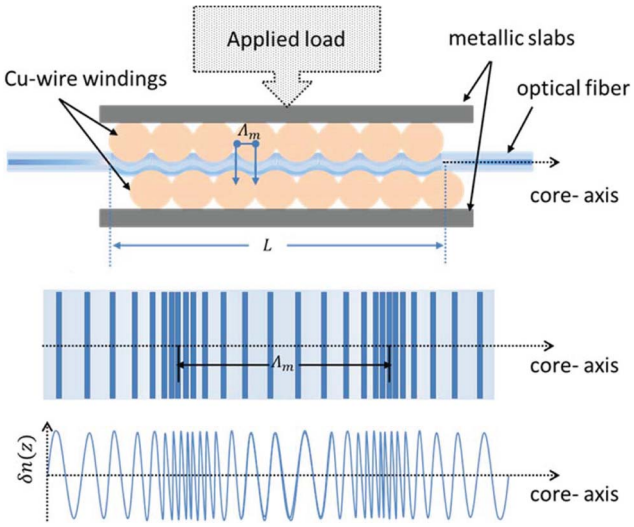

DOI: 10.1109/JPHOT.2013.2295466
1943-0655

IEEE photonics SOCIETY

IEEE

Optical Gaussian Notch Filter Based on Periodic Microbent Fiber Bragg Grating

M. M. Ali,[1] *Student Member, IEEE*, K. S. Lim,[1] *Member, IEEE*, A. Becir,[2] M. H. Lai,[1] and H. Ahmad[1]

[1]Photonics Research Centre, University of Malaya, 50603 Kuala Lumpur, Malaysia
[2]Faculty of Science and Arts, Shaqra University, 11961 Shaqra, Saudi Arabia

DOI: 10.1109/JPHOT.2013.2295466

Manuscript received October 27, 2013; revised December 4, 2013; accepted December 9, 2013. Date of publication December 20, 2013; date of current version December 27, 2013. This work was supported by the University of Malaya under HIR grant (UM.C/625/1/HIR/MOHE/SCI/29), UMRG Grant (RP019-2012C), (RU002/2013), and IPPP Grant (PG029-2013A). Corresponding author: K. S. Lim (e-mail: kslim@um.edu.my).

Abstract: In this paper, we demonstrated an optical notch filter constructed from a periodic microbent fiber Bragg grating attained by using two copper-wire-wound slabs. In the reflection spectrum, sideband peaks are created as a result of mechanically induced modulation on the grating period, and a higher number of peaks are observed when greater modulation is applied. The peak wavelength spacing depends upon the period of microbending, which can be varied by changing the diameter of the winding wire or the angle of placement of fiber Bragg grating placed in between the two wound slabs. Moreover, the trend of Bragg transmission loss (BTL) for the transmission spectrum changes with the changing of modulation period and amplitude. The proposed technique is very stable, and it can be used as an optical Gaussian notch filter.

Index Terms: Refractive index modulation, periodic microbending, Bragg wavelength, Bragg transmission loss.

1. Introduction

In the past few decades, there has been a growing interest in the study of fiber Bragg gratings (FBGs) and their applications in different areas e.g., stress, strain, temperature and pressure sensing and in many other applications of optical communication [1]. FBG comprises of a periodic refractive index modulation in the core of a single mode optical fiber, in which the phase fronts are perpendicular to the longitudinal axis of the fiber, also the accurate and direct measurement of gratings period can be done by using optical imaging technique proposed by [2]. By using the refractive index modulation property, many researchers have done a lot of research by introducing further modulation using the acousto-optic effect of the piezoelectric transducer (PZT) onto the core of FBG in order to make an acousto-optic modulator (AOM). The acousto-optic effect is used in the construction of several low insertion loss all-fiber devices, such as frequency shifters [3], modulators [4], Q-switched fiber lasers [5], and tunable narrow-bandwidth optical filters [6]. Applications of the AO effect that have been demonstrated so far are based either on the propagation of longitudinal or flexural acoustic waves in the optical fiber [7], [8]. The same effect can be achieved by the proposed method in this paper i.e., by mechanically inducing a periodic microbending of FBG. To our knowledge, this is the first study in which the mechanical microbending method for FBG has been proposed. The proposed method is very stable and easy to handle the adjustment issues by easily

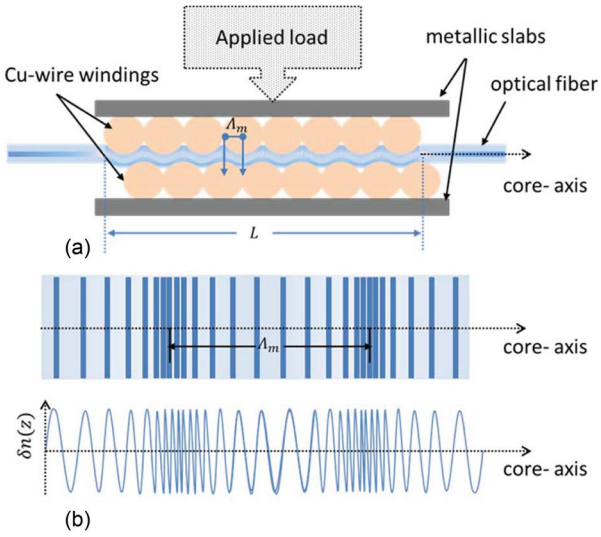

Fig. 1. (a) Experimental model diagram for micro-bending of FBGs. (b) Structural and graphical illustration of index modulation induced by micro-bending in optical fiber core.

controlling the applied load on metallic wound slabs in which FBG is placed in between them. When the load is applied, and due to alternative winding cycle of each slab, the microbending is induced. So the resulting index modulation profile of FBG is similar to the frequency modulation (FM), and multiple sideband peaks are produced in the reflection spectra. The theoretical model related to AOM has been discussed in detail by Russell *et al.* based on the superposition of an FBG and acousto-optic coupling between forward and backward photonic Bloch waves [9]. Later on, Oliveira *et al.* presented another theoretical model in which finite element method was used to investigate the acoustically induced strain field and the transfer matrix method for calculating the reflection spectrum of the acousto-optic modulator using FBG [7]. Despite the advantage of complete characterization of strain, the transfer matrix method requires large number of calculations and hence having low efficiency. So, to overcome this issue, Zhuoxuan Li *et al.* used the Fourier mode coupling (FMC) method for the first time in AOM analysis [10], and also the same theory has been used by Chao Liu *et al.* [11]. They have also reported that FMC model outperforms transfer matrix method in terms of computation efficiency while maintaining the accuracy. It has been observed that in the reflection spectra, the produced sidebands share Gaussian behavior i.e., the magnitude of central Bragg wavelength is maximum and fixed whereas the amplitude of sideband wavelengths decreases in similar way as the Gaussian curve. So the parameter of Gaussian curve width can be tuned by varying the diameter of winding wire or changing the angle of placement of FBG in between the slabs. In this investigation, the proposed optical Gaussian notch filter has the potential applications in optical communication such as suppressing the optical noises [12], [13], wavelength division multiplexing networks [14], and optical arbitrary waveform generation [15].

In the current study, FMC theory has been used to validate the experimental results that can be seen with good agreement. In Section 2, proposed analytical model is discussed in detail. In Section 3, the fabrication of Gaussian-apodization (GA) FBGs in the core of SMF-28 fiber and the experimental results for the reflection spectra of different configurations of microbending is described and it proves that the results are in good agreement with simulation results of analytical model. In addition, the Bragg transmission loss of FBG written in SMF-28 fiber with different microbending periods is presented. Finally, the conclusions are drawn in Section 4.

2. Mathematical Analysis of Proposed Technique

The proposed schematic model of experiment for microbending of FBGs is shown in Fig. 1(a). A non-uniform Gaussian apodized FBG has been used and the structural and graphical illustration of index modulation induced by micro-bending in optical fiber core is shown in Fig. 1(b).

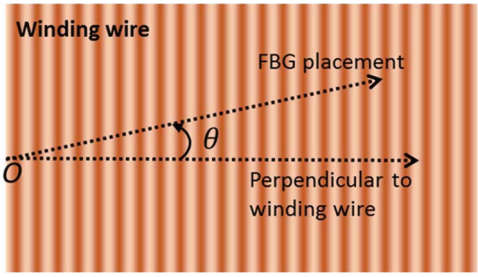

Fig. 2. Angle of placement (θ) of FBG placed in between the wound slabs.

The refractive index perturbation $\delta n(z)$ of the fiber core can be formulated as [16]

$$\delta n(z) = \delta n_0 \times \left\{1 + e^{\frac{-\alpha z^2}{L^2}} \sin\left(\frac{2\pi z}{\Lambda}\right)\right\}, \qquad |z| \leq L/2 \tag{1}$$

where δn_0 is the modulation depth of refractive index, α is the coefficient of Gaussian apodization for given fabricated FBG, L is the FBG length and Λ is the period of grating pattern along fiber core and z is the axis along the core of from FBG. When the periodic microbending is induced, the refractive index perturbation is related with microbending effect by using the concept frequency modulation (FM). So Eq. (1) can be modified as [9]

$$\delta n(z) = \delta n_0 \times \left\{1 + e^{\frac{-\alpha z^2}{L^2}} \sin\left(\frac{2\pi z}{\Lambda} + \frac{2\pi}{\Lambda}\int R\cos\left(\frac{2\pi z}{\Lambda_m}\right)dz\right)\right\}, \qquad |z| \leq L/2 \tag{2}$$

where R and Λ_m are the amplitude and period of mechanically induced microbending, respectively, as shown in Fig. 1. Further, R is proportional to the applied load, and Λ_m is proportional to the diameter of winding wire and inversely proportional to the term $\cos\theta$, where θ is the angle of placement of FBG in between the wound slabs, described in Fig. 2.

From the fundamental theory of optical waveguides, the coupling equation for FBGs can be derived easily using the Maxwell's differential equations for the forward and backward electromagnetic waves propagating inside the waveguide that is given by

$$\frac{dB_s(z)}{dz} = i\sum_m k_c B_m(z)\delta n(z) e^{-i(\beta_m+\beta_s)z} \tag{3}$$

where $i = \sqrt{-1}$ is complex number, m is the order of forward propagating mode, $B_m(z)$ and $B_s(z)$ are the amplitudes of forward and backward propagating fields modes, β_m and β_s are the propagation constants for the forward and backward propagating waves, respectively, while k_c is the mode coupling coefficient that is defined as

$$k_c = \frac{\epsilon_0 \omega n_0}{2} \iint_{A_{CS}} E_m(r,\phi) E_s^*(r,\phi)\, dA \tag{4}$$

where A is the cross-section area, A_{CS} is the total area, r and ϕ are the cylindrical coordinate axes, ω is the angular frequency, ϵ_0 is the permittivity of free space, n_0 is the core refractive index and E represents the electric field inside the fiber where asterisk $(*)$ shows the complex conjugate of electric field.

By applying phase matching condition, $\beta_m = \beta_s = (2\pi n_m/\lambda)$ and boundary conditions of FBG, the integration of Eq. (3) can be simplified. The integration term contains the expression of $\delta n(z)$ which can be considered exactly like Fourier transform that is decomposed in terms of real and imaginary parts as

$$\mathcal{F}(\delta n(z)) = \zeta(\Omega_m) + i\varsigma(\Omega_m) \tag{5}$$

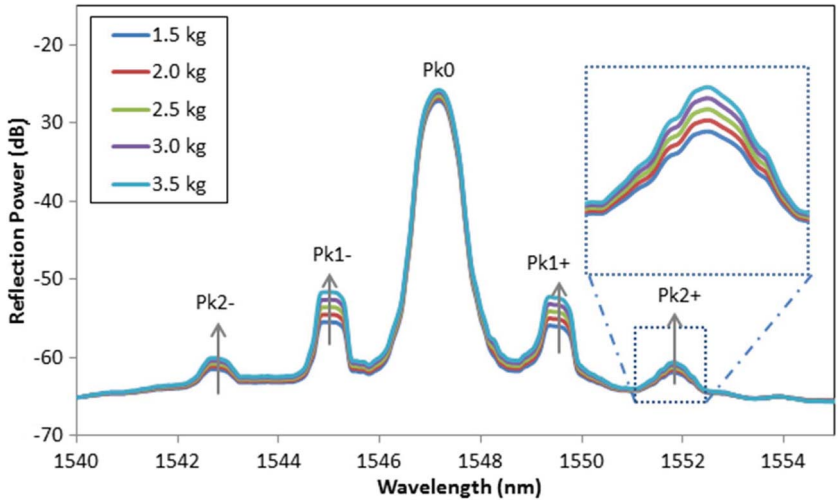

Fig. 3. The reflection spectrum of SMF-28 FBG under periodic microbending using thick wire and at different loads. Pk0 shows the central Bragg wavelength, Pk1+ and Pk2+ represent the first order sideband peak and second order sideband peak on right hand side of Pk0 respectivley and Pk1− and Pk2− represent the first order sideband peak and second order sideband peak on left hand side of Pk0 respectivley.

where $\mathcal{F}(\cdot)$ is the Fourier operator, $\zeta(\Omega_m)$ and $\varsigma(\Omega_m)$ are the real and imaginary part of transform respectively that are the function of $\Omega_m = (2n_m/\lambda)$. The real part on the right hand side of Eq. (5) is closer to zero for non-uniform Gaussian apodized FBG [11]. By applying some mathematical manipulations, we attain the following analytical expressions for reflection spectrum and transmission spectrum

$$\mathcal{R} = \frac{\cos^2(k_c\zeta)\sinh^2(k_c\varsigma) + \cosh^2(k_c\varsigma)\sin^2(k_c\zeta)}{\cos^2(k_c\zeta)\sinh^2(k_c\varsigma) + \cosh^2(1 + k_c\varsigma)\sin^2(k_c\zeta)} \tag{6}$$

$$\mathcal{T} = \frac{1}{\cos^2(k_c\zeta)\sinh^2(k_c\varsigma) + \cosh^2(1 + k_c\varsigma)\sin^2(k_c\zeta)}. \tag{7}$$

The Bragg transmission loss (BTL) is therefore given by K. S. Lim *et al.* [17]

$$BTL = 20\log_{10}\left\{\frac{\mathcal{T}_{background}}{\mathcal{T}(\lambda_{center})}\right\} \tag{8}$$

where $\mathcal{T}_{background}$ is the transmission power far from the center wavelength and $\mathcal{T}(\lambda_{center})$ is the transmission power at center Bragg wavelength.

3. Fabrication of FBG and Experimental Setup

The B-Ge co-doped standard optical fiber SMF-28 was used for the fabrication of FBG. For the fabrication of FBG on H_2 loaded fiber, the FBG structure was inscribed into the fiber core by KrF_2 excimer laser based on fixed beam phase mask technique. The Gaussian laser beam was expanded from ∼0.6 cm to ∼2.0 cm using a beam expander and thus it can produce Gaussian apodized FBGs of about the same length. After the fabrication, FBGs were annealed in a hot oven at 80 °C for 10 hours to remove the residue hydrogen gas in the FBGs to stabilize the center Bragg wavelengths and *BTL*. After writing FBG, the periodic microbending of FBG has been carried out using experimental setup shown in Fig. 1. The length of all FBGs that have been used in experiment is ∼2.0 cm. and for bending, the Copper (Cu) wire of two different diameters has been used i.e., thin wire of diameter ∼0.2 mm and thick wire of diameter ∼0.3 mm. As the FBG was placed in between the copper wound metal slabs, some precautions have been taken to avoid the breakage of the uncoated FBG. First precaution is that the metallic wire should be wound tightly on metallic cubical

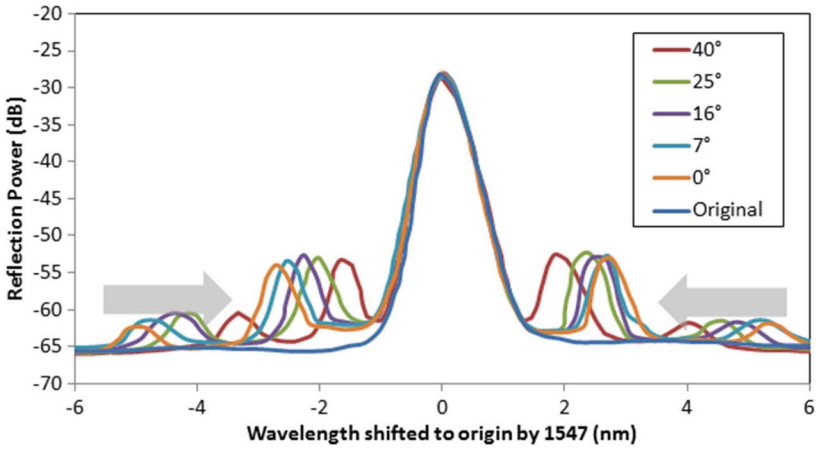

Fig. 4. The reflection spectrum of FBG under periodic microbending using thick wire by varying angle of placement as $\theta = 0^\circ$ 7°, 16°, 25°, and 40°.

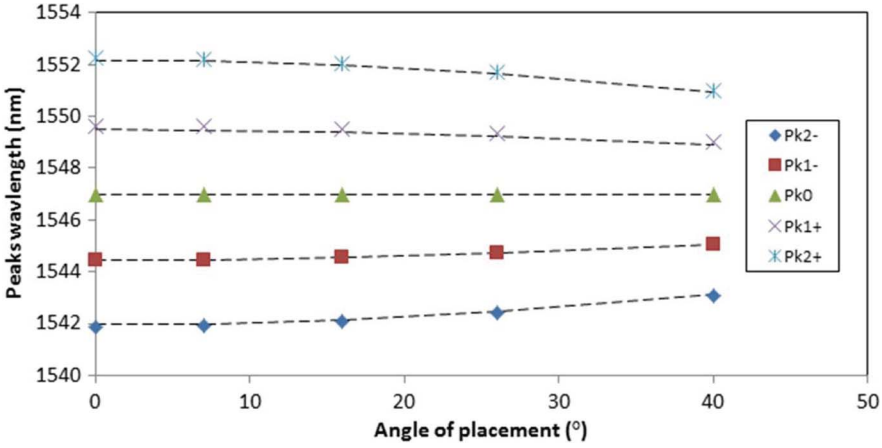

Fig. 5. The peak positions of central Bragg wavelength and of sideband peak wavelengths of FBG under periodic microbending using thick wire at different angle of placement. Dotted curves represent the simulation result.

slab so that there should be no space in between the winding loops to prevent any excessive microbending at any local point along the fiber. Another precaution is that the load should be applied at centre of the wound slabs so that the applied force is distributed uniformly along the fiber.

The period of microbending Λ_m is considered as the function of angle of placement (θ), where the fiber placement exactly perpendicular to the windings has been considered at 0° angle as shown in Fig. 2. The function Λ_m is written as

$$\Lambda_m = \frac{d}{\cos\theta} \tag{9}$$

where d is the diameter of winding wire. It is clear that by increasing the angle the period of microbending will also increase and in result at $\theta = 90^\circ$ there will be no microbending i.e., the fiber will be parallel with winding wire.

3.1. Experimental and Simulation Results With Discussions

In this subsection the experimental and simulation results are being discussed. Figs. 3–5 show the results for thick wire winding. Fig. 3 shows the reflection spectrum of FBGs written in SMF28

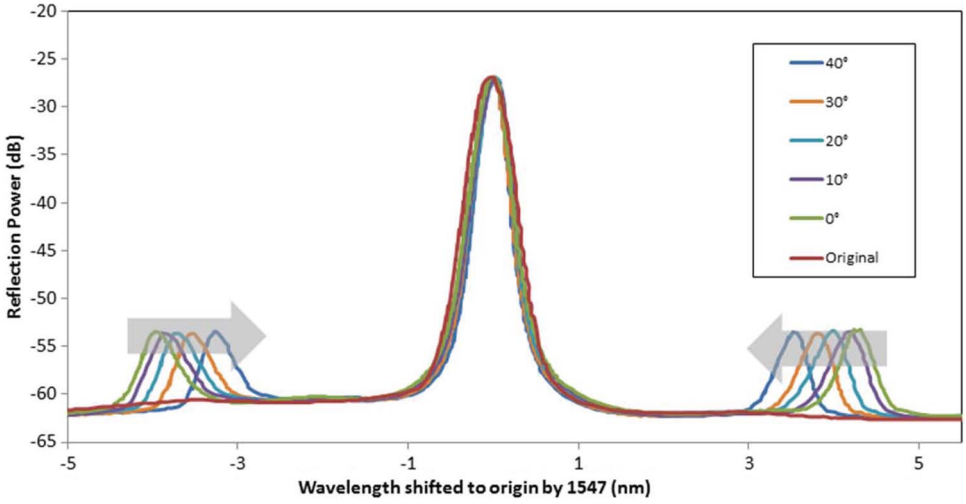

Fig. 6. The reflection spectrum of FBG under periodic microbending using thin wire by varying angle of placement as $\theta = 0^\circ$ 10°, 20°, 30°, and 40°.

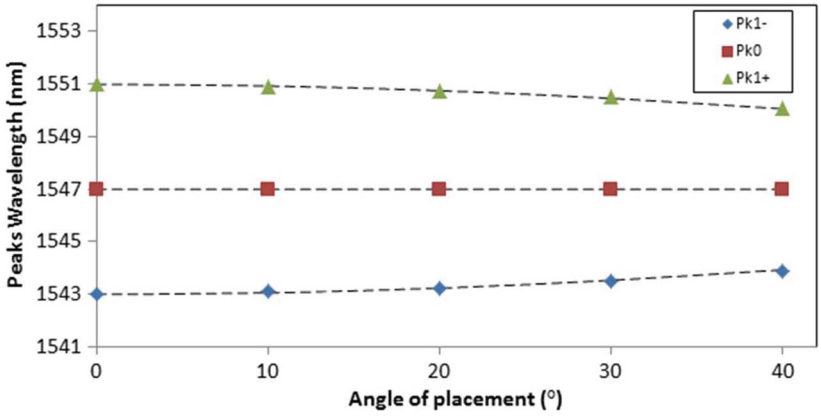

Fig. 7. The peak positions of central Bragg wavelength and of sideband peak wavelengths of FBG under periodic microbending using thin wire at different angle of placement. Dotted curves represent the simulation result.

under periodic microbending using thick wire by varying loads. From Fig. 3, it is clear that when the load is applied on the slab the microbending effect increases eventually the sideband peaks i.e., first order peaks (Pk1+ and Pk1−), second order peaks (Pk2+ and Pk2−) and so on, appear that are proportional to the applied load on the upper slab. The peaks power profile looks like Gaussian curve centered at the Bragg wavelength.

Fig. 4 shows that when the load is fixed and the angle of placement is incremented from 0°, the sideband wavelengths approaches the central Bragg wavelength. From Fig. 5, it is clear that the shift of second order sideband peaks is greater than the shift of first sideband peaks. The markers in Fig. 5 represent the peaks position of the periodic microbent FBG and they are in good agreement with the calculated results from FMC theory.

The same experiment is carried out using thin wire and the results are presented in Figs. 6 and 7. From Fig. 6, it is clear that only the first order sidebands are visible while the second order sidebands cannot be seen in the spectrum because of their larger wavelength spacing from the central Bragg wavelength and they have lower reflected power than the ASE noise level. This indicates that the wavelength spacing between the sidebands and the central Bragg wavelength is governed by the modulation period or the diameter of the winding wire in which smaller wire

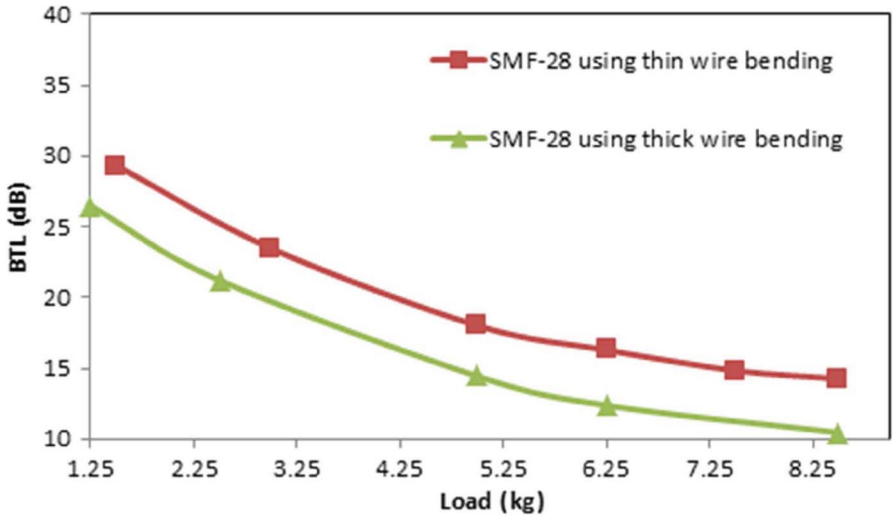

Fig. 8. The relationship between Bragg transmission loss of periodic microbent SMF-28 FBGs and load.

diameter yields larger wavelength spacing. The similar trend can be observed when the FBG is placed with different angles in between the slabs wound by thin wire i.e., the peaks shift towards the central Bragg wavelength as shown in Fig. 7. From the reflection spectrum, it can be seen that it has a Gaussian envelope whose sideband wavelengths can be controlled, by tuning angle of placement or by changing the winding wire. However, the central Bragg wavelength is unaffected by the microbending.

Fig. 8 shows the relationship between *BTL* and the applied load on an FBG with an initial *BTL* of 32.0 dB. The results for two different configurations, namely thin wire and thick wire wound slabs used in the investigation are presented. In comparison, for the case of thick wire, the FBG had suffered greater drop in *BTL* because of the larger wire diameter and the fiber underwent a great change in the fiber physical structure when the first load of 1.25 kg was applied. However, the rate of decrement in *BTL* with increasing the load for the two configurations are the same. This indicates that there was no further significant change in physical structure but merely some increment in pressure and strain applied on the FBG, which can be interpreted as microbending modulation amplitude *R*.

4. Conclusion

In conclusion, the spectral characteristics of fiber Bragg grating under periodic microbending have been studied theoretically and experimentally. Simple analytical equations have been derived to describe the reflection and transmission spectrum of periodic microbent FBG using Fourier mode coupling theory and also the *BTL* of different fibers have been investigated which is completely in agreement with results reported in literature. Our finding indicates that the grating strength degrades with the increasing bending loss. It has been shown that the gap between sideband wavelengths and central Bragg wavelength depends upon the period of microbending, which can be tuned by changing the diameter of metallic winding wire or changing the angle of placement in between the wound slabs. The proposed technique is very stable and can be used as Optical Gaussian notch filter.

References

[1] A. Gillooly, "Photosensitive fibers: Growing gratings," *Nature Photon.*, vol. 5, pp. 468–469, 2011.
[2] M. M. Ali, K. S. Lim, H. Z. Yang, W. S. Chong, and H. Ahmad, "Direct period measurement for fiber Bragg grating using an optical imaging technique," *Appl. Opt.*, vol. 52, no. 22, pp. 5393–5397, 2013.

[3] B. Y. Kim, J. N. Blake, H. E. Engan, and H. J. Shaw, "All-fiber acousto-optic frequency shifter," *Opt. Lett.*, vol. 11, no. 6, pp. 389–391, 1986.
[4] H. F. Taylor, "Bending effects in optical fibers," *J. Lightw. Technol.*, vol. 2, no. 5, pp. 617–628, Oct. 1984.
[5] M. Delgado-Pinar, D. Zalvidea, A. Díez, P. Pérez-Millán, and M. V. Andrés, "Q-switching of an all-fiber laser by acousto-optic modulation of a fiber Bragg grating," *Opt. Exp.*, vol. 14, no. 3, pp. 1106–1112, Feb. 2006.
[6] D. I. Yeom, H. S. Park, and B. Y. Kim, "Tunable narrow-bandwidth optical filter based on acoustically modulated fiber bragg grating," *IEEE Photon. Technol. Lett.*, vol. 16, no. 5, pp. 1313–1315, May 2004.
[7] R. A. Oliveira, P. T. Neves, Jr., J. T. Pereira, and A. A. P. Pohl, "Numerical approach for designing a Bragg grating acousto-optic modulator using the finite element and the transfer matrix methods," *Opt. Commun.*, vol. 281, no. 19, pp. 4899–4905, Oct. 2008.
[8] W. F. Liu, I. M. Liu, L. W. Chung, D. W. Huang, and C. C. Yang, "Acoustic-induced switching of the reflection wavelength in a fiber Bragg grating," *Opt. Lett.*, vol. 25, no. 18, pp. 1319–1321, Sep. 2000.
[9] P. St. J. Russell and W.-F. Liu, "Acousto-optic supperlattice modulation in fiber Bragg gratings," *J. Opt. Soc. Amer. A*, vol. 17, no. 8, pp. 1421–1429, Aug. 2000.
[10] Z. X. Li, L. Pei, C. Liu, T. G. Ning, and S. W. Yu, "Research on FBG-based longitudinal-acousto-optic modulator with Fourier mode coupling method," *Appl. Opt.*, vol. 51, no. 30, pp. 7314–7318, Oct. 2012.
[11] C. Liu, L. Pei, Z. Li, T. Ning, S. Yu, and Z. Kang, "Spectra analysis of non-uniform FBG-based acousto-optic modulator by using Fourier mode coupling theory," *Appl. Opt.*, vol. 52, no. 14, pp. 3318–3323, May 2013.
[12] A. Ghazisaeidi, F. Vacondio, and L. A. Rusch, "Filter design for SOA-assisted SS-WDM systems using parallel multicanonical Monte Carlo," *J. Lightw. Technol.*, vol. 28, no. 1, pp. 79–90, Jan. 2010.
[13] M. V. Drummond, A. Ferreira, T. Silveira, D. Fonseca, R. N. Nogueira, and P. Monteiro1, "Optimization of a FBG-based filtering module for a 40 Gb/s OSSB transmission system," *Opt. Appl.*, vol. 40, no. 2, pp. 511–520, 2010.
[14] P. L. Chu, B. A. Malomed, and G. D. Peng, "Soliton WDM system using channel-isolating notch filters," in *Proc. SPIE 3847, Opt. Devices Fiber Commun.*, 1999, vol. 3847, pp. 158–165.
[15] Z. Jiang, C. B. Huang, D. E. Leaird, and A. M. Weiner, "Optical arbitrary waveform processing of more than 100 spectral comb lines," *Nature Photon.*, vol. 1, pp. 463–467, 2007.
[16] R. Kashyap, *Fiber Bragg Gratings*. New York, NY, USA: Academic, 1999.
[17] K. S. Lim, H. Z. Yang, A. Becir, M. H. Lai, M. M. Ali, X. G. Qiao, and H. Ahmad, "Spectral analysis of bent fiber Bragg gratings: Theory and experiment," *Opt. Lett.*, vol. 38, no. 21, pp. 4409–4412, Nov. 2013.